Probabilistic Bridge Fatigue Evaluation at Virtual Sensing Locations using Kernel Density Estimation

Article *in* International Journal of Fatigue · August 2023

DOI: 10.1016/j.ijfatigue.2023.107885

3 authors, including:

Emmanuel Akintunde
University of Nebraska at Lincoln
8 PUBLICATIONS **22** CITATIONS
SEE PROFILE

Saeed Eftekhar Azam
University of New Hampshire
77 PUBLICATIONS **1,568** CITATIONS
SEE PROFILE

International Journal of Fatigue xxx (xxxx) 107885

Contents lists available at ScienceDirect

International Journal of Fatigue

journal homepage: www.elsevier.com/locate/ijfatigue

Probabilistic bridge fatigue evaluation at virtual sensing locations using kernel density estimation

Emmanuel Akintunde [a,*], Saeed Eftekhar Azam [b], Daniel G. Linzell [c]

[a] Olsson Inc., Omaha, NE, USA
[b] Department of Civil and Environmental Engineering, University of New Hampshire, Durham, NH, USA
[c] Department of Civil and Environmental Engineering, University of Nebraska-Lincoln, Lincoln, NE, USA

ARTICLE INFO

Keywords:
Strain estimation
Singular value decomposition
Self-organizing map
K-means clustering
Railway bridge
Virtual sensing
Kernel density estimation
Reliability analysis
Monitoring data
Fatigue assessment

ABSTRACT

Performing bridge fatigue evaluation using field measurements can be difficult given the amount of data needed for effective assessment, access needed to effectively monitor all fatigue prone locations, and associated power requirements and cost. Several studies have been conducted that estimate strain response at unmeasured locations using indirect measurements and subsequently investigate the quality of the estimation using certain metrics [1]. There is little to no research focusing on pragmatically extending these estimation techniques to probabilistic fatigue assessment. This may be because strain estimation has primarily been successful when applied to numerical and laboratory specimens and perceived potential for difficulties associated with applying developed techniques at scale. This study investigates using data-driven, Singular Value Decomposition (SVD), estimated strains at unmeasured locations for probabilistic fatigue assessment of an in-service, railway, bridge. Before performing strain estimations, SVD Proper Orthogonal Modes (POM) variability was reduced using two classification approaches: k-means clustering and root mean square (RMS); and self-organizing maps (SOMs) and POMs. After estimated strains were obtained, reliability analyses using Kernel Density Estimation (KDE) were utilized to perform probabilistic fatigue assessments. Resulting reliability indices computed using estimated strains were compared against reliability indices obtained using measured strains at the same locations. Results showed that reliability indices computed using estimated strains matched closely with indices obtained using measured strains.

1. Introduction

Performing accurate probabilistic fatigue assessment of an in-service bridge using response measurements can be difficult due to insufficient data. One of the major factors limiting the amount of data that can be obtained from a bridge is inaccessibility to myriad fatigue prone locations needing direct measurements from physical sensors [2]. For cases where access is not as difficult and sensors can be appropriately placed, a limited number of locations can be monitored due to sensor cost and power requirements [3]. To address this issue, virtual sensing research studies have been carried out to estimate strain response of structures at unmeasured locations via indirect measurements. Successful estimations were obtained for a range of civil, offshore, and mechanical structures [4–6]. However, most applications have been limited to numerical and laboratory specimens.

Virtual sensing can be classified as either model-based (analytical), data-based (empirical), or a combination of the two [7]. For model based virtual sensing, Kalman Filtering (KF) and Modal Expansion (ME) are two commonly used strain estimation processes [7]. Both KF and ME allow for estimation of an unmeasured response using sparsely measured time history response and a physics model, such as finite element model [8,9].

Comparisons between KF and ME algorithm response estimation effectiveness have been performed [4,10–12]. Ren and Zhou [4] investigated the accuracy and efficiency of both algorithms for predicting strain response at unmeasured locations on a steel truss using limited actual measurements and a FE model. Both algorithms produced good predictions. Given that both methods are model/physics-based, requiring calibration of an FE model to determine modal parameters for strain estimation can be tedious, especially for large and complex structures. These limitations triggered studies investigating data-driven methods for strain estimation [13,14].

Azam et al. [15] recently introduced novel application of data driven SVD to predict strain response for an in-service steel railway bridge

* Corresponding author.
E-mail address: eakintunde@olsson.com (E. Akintunde).

https://doi.org/10.1016/j.ijfatigue.2023.107885
Received 9 December 2022; Received in revised form 8 August 2023; Accepted 10 August 2023
0142-1123/© 20XX

monitored using a sparse sensor network. Strain response at measured locations from two train passages was stored in a snapshot matrix and left singular vector (LSV) modes from SVD of snapshot matrices, known as Proper Orthogonal Modes (POMs), were utilized for strain estimation instead of vibration modes from a FE model for ME strain estimation. The developed data-driven SVD method was compared against results from model-based methods that used augmented KF and ME. Examined methods produced accurate strain estimations and proved to be adequate virtual sensing tools for continuous health monitoring, with SVD outperforming augmented KF and ME. It was also stated that SVD can be seamlessly applied to linear and nonlinear systems and does not need any information related to external loads (e.g., train axle loads and length), loaded track, and the direction and speed of the train.

A recent study [16] by the authors contains a detailed discussion of the developed data driven SVD method using data from many train passages. It was shown that POM variability resulting from larger data sets could significantly affect strain estimation accuracy. POM variability was reduced using two proposed classification methodologies: (1) k-means clustering and RMS, and (2) classification using Self Organizing Maps (SOMs) and POMs. Using these methods, measured strain responses were clustered into groups of trains with similar loads and speeds moving in the same direction, POM variability was reduced, and improved strain estimations occurred.

While extensive research into strain estimation on several different types of structures using various numerical techniques have occurred, limited research that attempts to utilize estimated response for performing fatigue assessment at unmeasured locations is available. Confidently identifying fatigue-prone zones on bridges using minimal sensors could be of great benefit to the bridge industry and to structural health monitoring. Leveraging findings from [16], this study investigates and compares the accuracy of fatigue assessment results at what are assumed unmeasured locations on an in-service steel railroad bridge to actual measurements at those locations. This investigation helped ascertain risks associated with using estimated response for fatigue evaluation. To perform the fatigue assessment, a proposed reliability analysis methodology employing Kernel Density Estimation (KDE) was utilized. KDE was employed to overcome challenges associated with selecting appropriate probability distributions to fit equivalent stress range distributions as KDE directly addresses statistical uncertainties that may be introduced.

2. Estimated strain with singular value decomposition

Data driven SVD was utilized to estimate strain response at unmeasured locations on the monitored steel, railroad, bridge. To reduce POM variability observed during the 2-month monitoring period, before strain estimation occurred two classification methodologies were employed to group measured strain response into classes of trains moving in same directions having similar loads and speeds.

2.1. Monitored bridge

The examined bridge is a fully operational, open deck, double-track, multi-span truss and through girder riveted steel railway bridge in central Nebraska. A single, 44.7-meter-long, simply supported truss span was monitored as shown in Fig. 1. The floor system employed seven transverse floor beams and four longitudinal stringers spaced 2.15 m center to center to support timber railroad ties (Fig. 2). In the figure, U1-U5 and L0-L6 are panel points on the upper and lower chords of the truss, respectively. L*X*N and L*X*S represent lower chord panel point L*X* on the north and south truss and FB*X* represents a floor beam between the same lower chord points.

Twenty Bridge Diagnostic Inc. (BDI) strain transducers were mounted on stringer bottom flanges close to the floor beams to obtain live load response, as fatigue of the stringer to floor beam connections can be of significant concern for many riveted steel bridges. Strain transducer locations on the truss floor system are presented in Fig. 3 with transducers numbered indicated. Areas in the red box (Sensors 16 – 20) were presumed to be unmeasured locations for strain estimation purposes using measured response data from “measured” locations in the blue box (Sensors 1 – 15). The authors were unable to instrument locations with the highest stress concentrations (e.g., rivet holes and the connection angles) during monitoring. However, the proposed SVD framework was implemented using the existing sensor network to estimate strains and compare estimates to the actual measurements. It is important to highlight that the proposed framework could be easily implemented for locations having high stress concentrations. Estimates

Fig. 1. Monitored truss span.

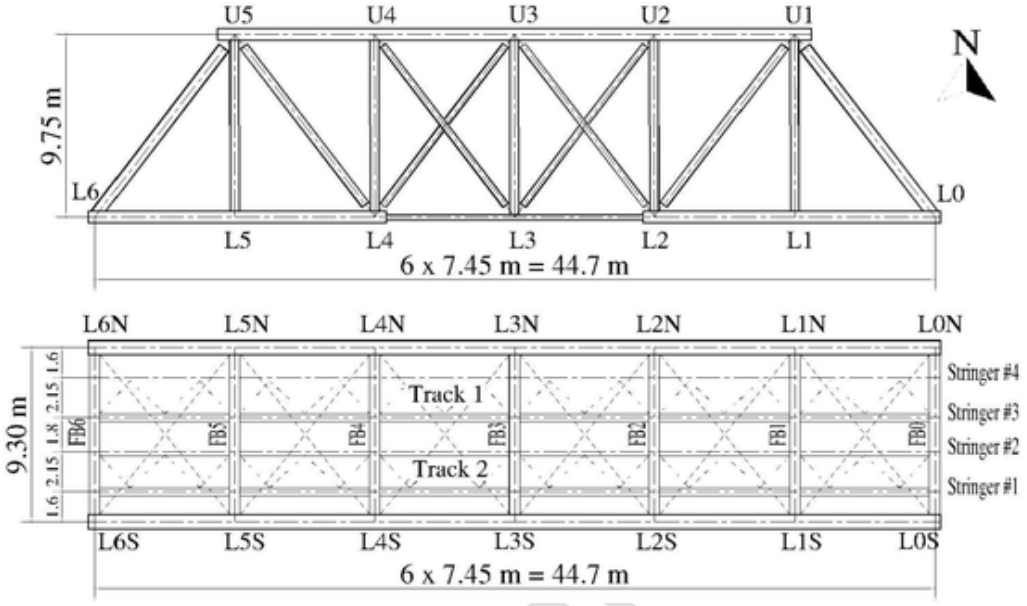

Fig. 2. Truss elevation and plan view.

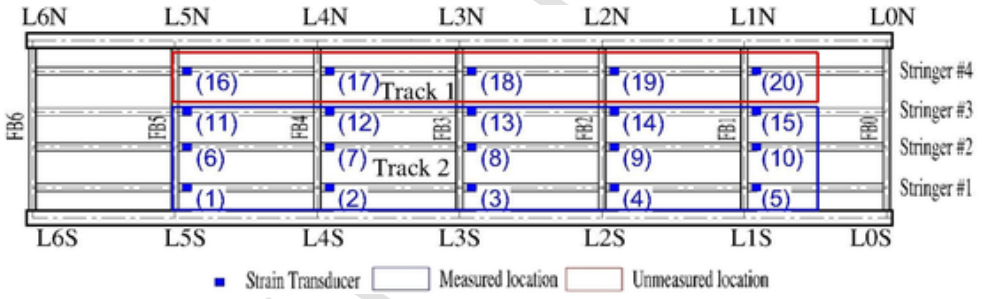

Fig. 3. Truss floor system instrumentation plan.

from the developed reliability-based, fatigue assessment process at the unmeasured locations were validated against results from actual measurements at those locations.

Fig. 4 and Fig. 5 show the strain time history captured during the monitoring period at Sensor 13 for one train passage on Track 1 and the equivalent stress-range histogram for the monitoring period at the sensor, respectively. Due to partial fixity at the connections, relatively small stress ranges are observed in Fig. 5.

2.2. Classification using k-means clustering and RMS

Azam et al. [17] established that the RMS of strain time-histories from a train passage were strongly correlated to that train's statically equivalent uniform load (i.e., input). As expected, when loads increased the magnitude RMS for each strain signal also increased. This relationship was further explored to ascertain which track the train was on when it traversed the bridge, with the track having the higher RMS value being equated to the one carrying the train. As shown in Fig. 3, RMSs from Sensors 1–5 at the south side of Track 2 were compared to those from Sensors 11–15 on the south side of Track 1. Fig. 6 presents snapshot matrix POMs from the 1852 train passages during the 2-month monitoring period and differentiates POMs from trains on Track 1 from those for trains on Track 2. There was a total of 967 train passages on Track 1 and 885 train passages on Track 2. Using these classifications reduced POM variations by eliminating train location uncertainty.

K-means clustering was utilized to further reduce POM variations by subdividing strain RMSs from each track snapshot matrix into four clusters. K-means clustering is an unsupervised machine learning technique that splits a set of n observations into k clusters by grouping data with similar underlying patterns [18]. It is a commonly used clustering algorithm because of low computational cost, simplicity, ease of implementation, and accuracy [19]. The sum of squared distances between observations and the cluster's centroid, which is the arithmetic mean of all data points belonging to that cluster, is minimized, and grouping is achieved by allocating every observation to its nearest cluster. Each observation can only be allocated to one cluster and the less variation within a cluster, the more similar the data points. Strain response from each cluster was used for strain estimation. Additional subcategorization of train passages by track further minimized POM dispersion, which enhanced strain estimation accuracy.

It is difficult to obtain more information about applied load characteristics in terms of the type of freight cars traversing a bridge. To mitigate this issue, the authors came up with a way to classify train loads using measured strain data. In a previous research work [20], the authors showed that there is strong correlation between train axle weights and RMS of measured dynamic strain. Hence, the average RMS for all sensors for each train passage was computed, sorted, and subcategorized into four classes (i.e., groups) that represent train loads categories using k-means clustering as shown in Fig. 7. Average RMS was used to represent each train passage since only a single RMS value is required for k-means clustering. These classes represented 'light' trains (Class 1), 'moderate' trains (Class 2), 'heavy' (Class 3), and 'extremely

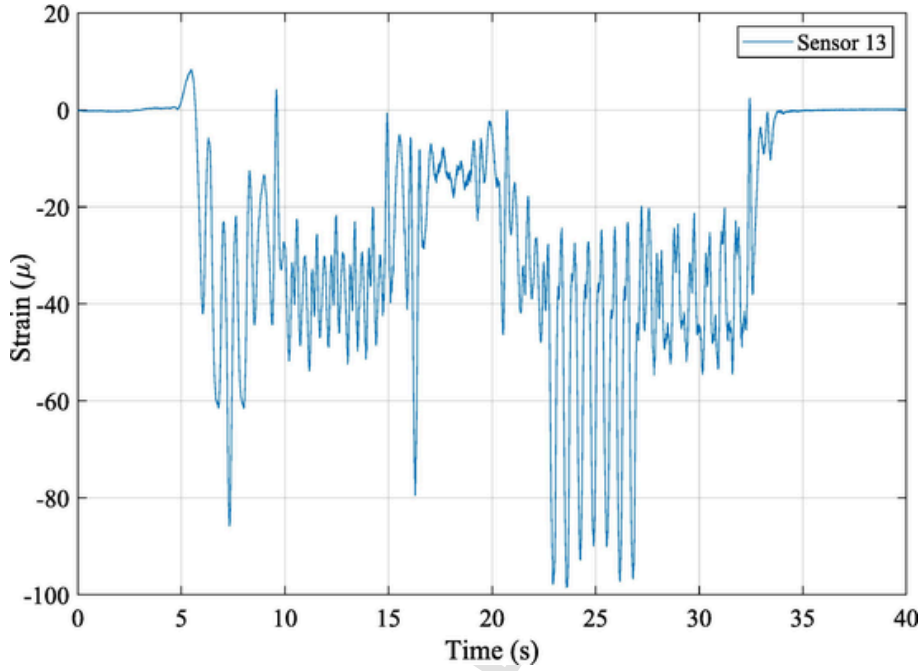

Fig. 4. Sensor 13 strain time-history, train passage on Track 1.

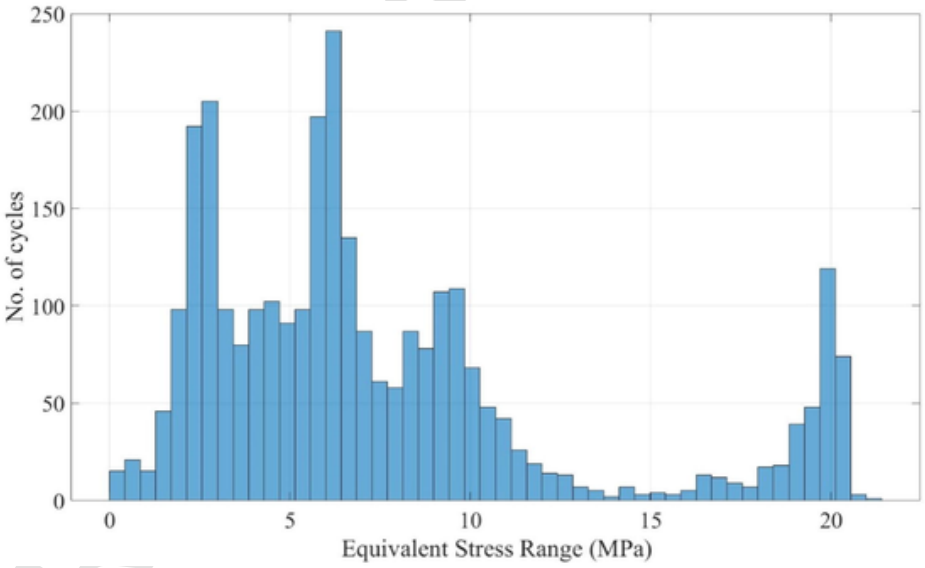

Fig. 5. Sensor 13 equivalent stress range.

heavy' (Class 4), with these categories being arbitrarily defined. The strain response at unmeasured locations in a class as depicted in Fig. 7 was subsequently estimated using measured strain POMs from all passes in that class. More details about the strain estimation computational process are presented in [15]. Readers interested in more details about freight cars characteristics are referred elsewhere [21–25].

Fig. 8 depicts representative estimated and measured strain response time-histories at unmeasured locations from Fig. 3 for a Class 4 train passage on Track 1. Class 4 was selected to show strain time-histories from a higher load category. Estimated time histories closely match measured responses at each location.

2.3. Classification using Self organizing maps and POMs

SOM is widely applied to clustering applications in industry, finance, natural science, and linguistics [26] as it clusters data while retaining original topology. SOM employs a network of connected neurons to determine Euclidean distances between each neuron and corresponding input data to determine a "winning" neuron. The winning neuron has a weight vector that is the closest to actual input data pattern, with the weight vector being tuned to both the input pattern and adjacent neurons [27]. The adoption of SOM over other techniques for the current study was justified based upon its robust dimensionality reduction and grid clustering capabilities, which facilitate data visualization, interpretation, and pattern recognition [28].

MATLABs *Neural Network Clustering App* [29] was utilized to implement SOM as the app creates, visualizes, and trains the network. A sin-

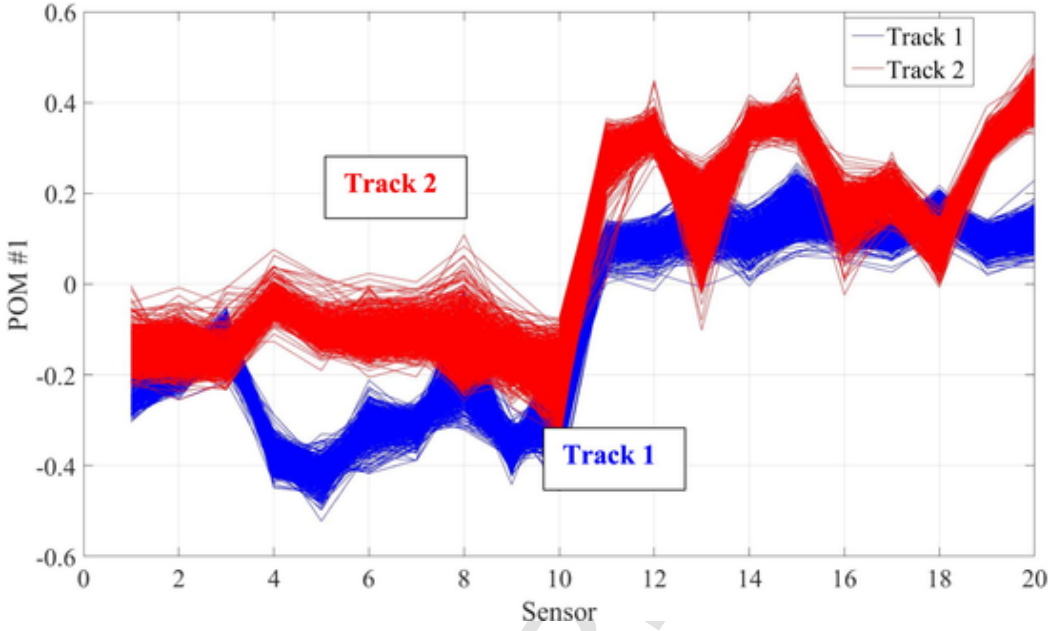

Fig. 6. RMS categorization of train passages POMs based on transverse track.

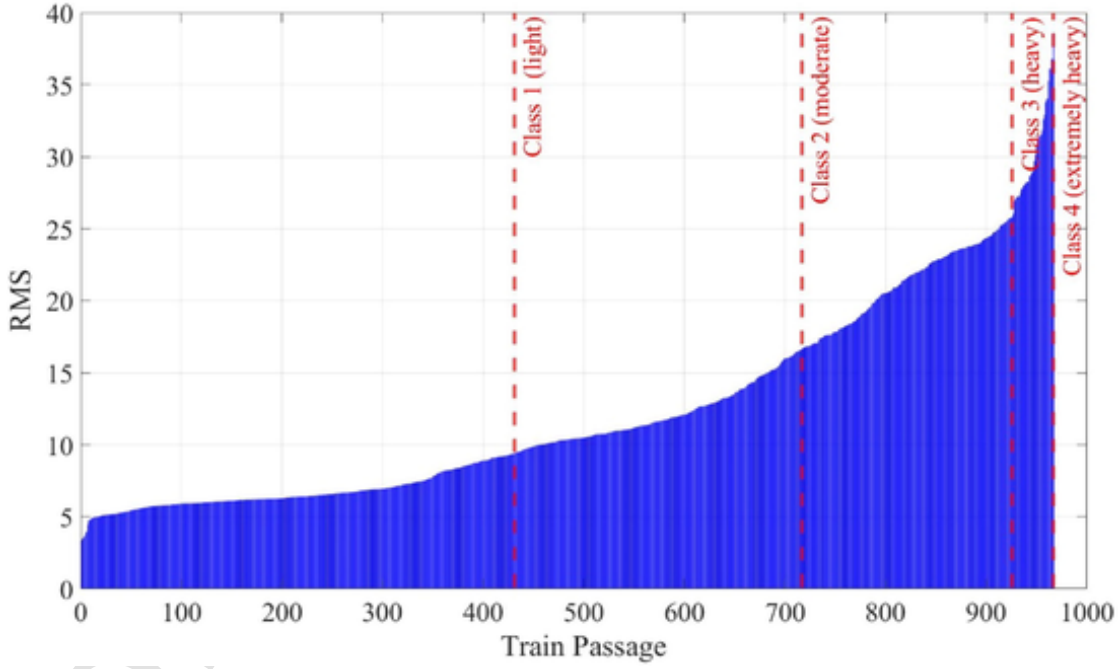

Fig. 7. Average RMS sub-categorization using k-means clustering.

gle layer of grid-like SOM neurons learns to cluster data based on similarity. The neural network is trained when data is imported and is defined by specifying a two-dimensional map of size n that corresponds to n^2 output clusters (i.e., n rows by n columns). A map size of $n = 1,2, 3..., k$ corresponds to an output of $1,4, 9..., k^2$ clusters, respectively. A minimum map size of '2′ is recommended.

POMs from all train passage snapshot matrices were imported into the clustering app, and a map size of '2′ was defined, yielding 4 clusters. As shown in Fig. 9, the number of observations (POMs) connected with each of the 4 cluster neurons is stored and displayed in a SOM sample hit, which is a graphical presentation of the number of input observations classified in each neuron. The number in a colored patch indicates the proportional number of observations for each neuron. Neurons are graphically arranged in a hexagonal pattern with x and y axes describing the position of each neuron on the grid for easy identification. It was observed that POMs were mostly grouped into two clusters/hits (967 and 885) with the others being empty. Akin to RMS characterization, these results demonstrate that the train was on either Track 1 (Hit 1 = 967) or Track (Hit 2 = 885). This preliminary clustering is analogous to classification of train passages based on location discussed in the previous section and, again, reduces POM dispersion.

Train passages were further sub-categorized into the 4 classes outlined previously using k-means clustering and RMS. The goal of the second sub-categorization was to again reduce POM dispersion resulting from loads and a SOM map size of '2′ was used. As indicated in Fig. 10 and Fig. 11, train passages were subcategorized into classes for Tracks 1

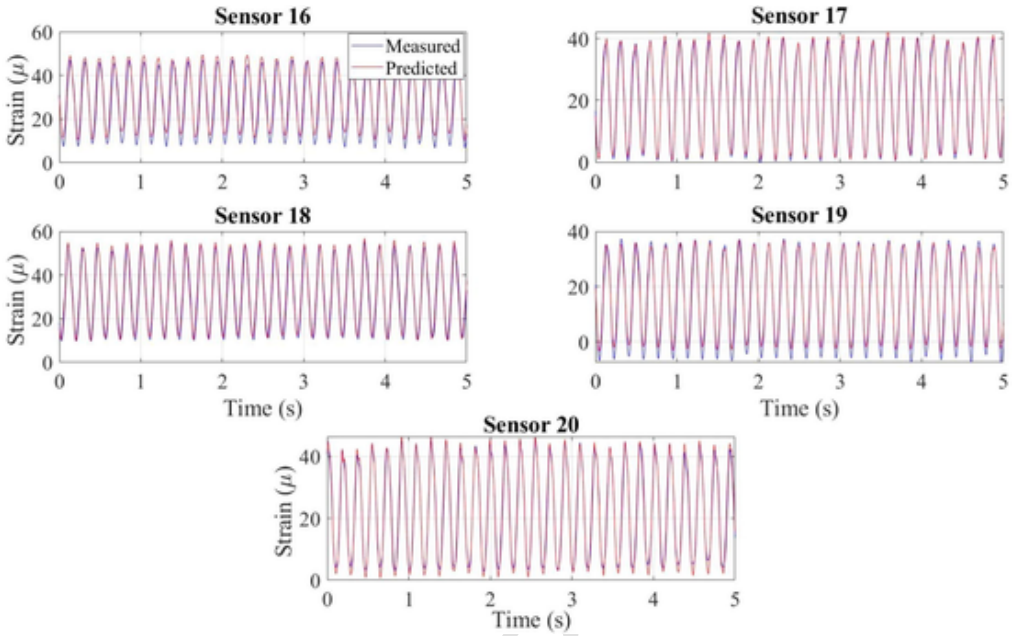

Fig. 8. RMS classification: predicted and measured strain time-histories for Class 4 (extremely heavy) train passages on Track 1, Sensors 16—20 (Fig. 3).

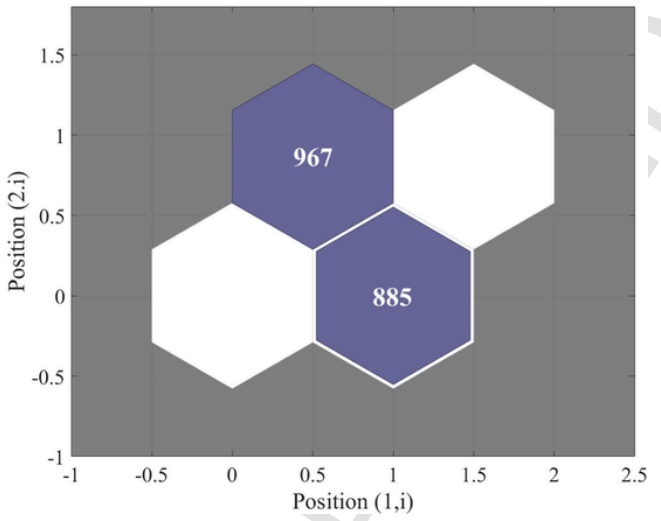

Fig. 9. Sample SOM hits from neural network clustering of train passage POMs; Hit 1 = Track 1, Hit 2 = Track 2.

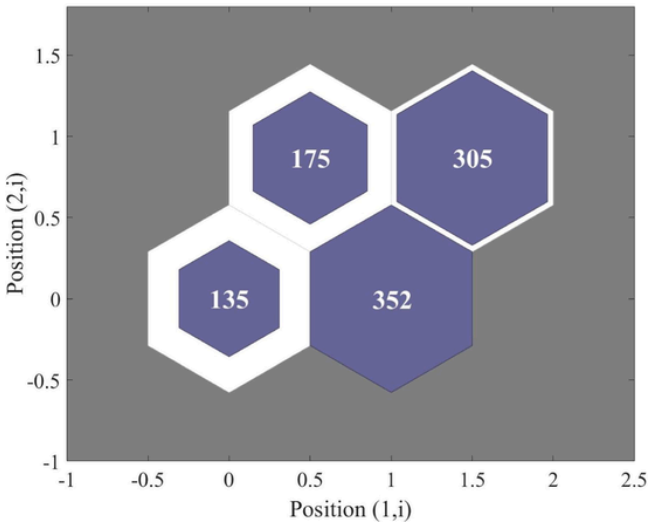

Fig. 10. Sample SOM hits from neural network clustering of train passage POMs, Track 1.

and 2, respectively. However, while clear classifications were evident, given the results it was difficult to independently determine which classes related to defined train load categories using SOM classification.

Having reduced POM variations somewhat via preliminary and secondary classifications, strains from the four classes were estimated using POMs and used to predict unmeasured location strain time-histories for the same class. Having shown representative strain time-histories from the higher load category (Class 4) previously, a representative plot from a lower load category (Class 1) is shown here. Fig. 12 shows a portion of the estimated and measured strain time history for a Class 1 (light) train passage on Track 2. Results indicate that the estimated time histories closely match measured responses at each location.

3. Fatigue assessment with estimated strain at unmeasured locations

After estimating strain response at unmeasured locations using RMS and SOM, fatigue assessment was performed using estimated strains and a reliability analysis methodology. Findings were compared against similar results from actual data at these locations to investigate the efficacy of using estimated strains to help identify fatigue prone locations. Reliability analysis using Kernel Density Estimation (KDE) was employed because it eliminates difficulty associated with choosing an appropriate distribution for equivalent stress range time histories at various connections, making it an efficient and accurate method for predicting remaining fatigue useful life.

KDE eliminates difficulty associated with selecting a suitable parametric distribution to represent a variation in data, such as equivalent stress range. Suppose a structure with resistance R is loaded with m loads, Q. A limit state function, M, can be defined as follows:

$$M = g(R, Q) = R - \sum_{i=1}^{m} Q_i \quad (1)$$

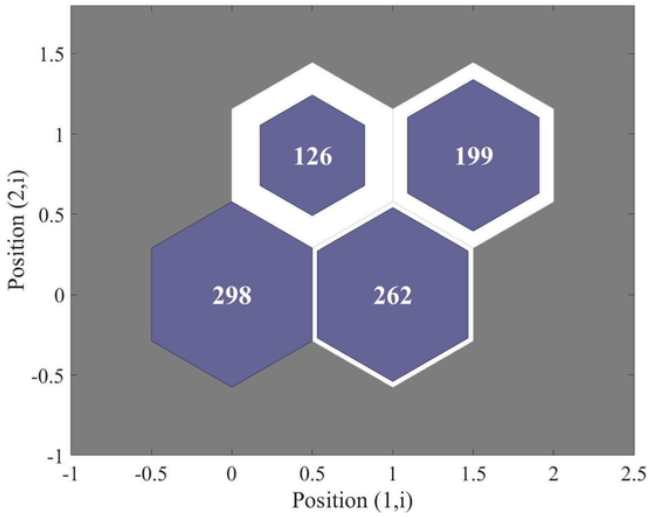

Fig. 11. Sample SOM hit from neural network clustering of train passage POMs, Track 2.

For an n-dimensional vector of constants $\mathbf{a^T} = [a_1, a_2, a_3, \cdots, a_n]$ and random variables, $\mathbf{X} = [X_1, X_2, X_3, \cdots, X_n]^T$, the limit state function in Eqn. (1) can further be expressed as follows:

$$M = a_1X_1 - (a_2X_2 + a_3X_3 + \ldots + a_nX_n) = \mathbf{a^TX} \tag{2}$$

where a_1X_1 represents the resistance, R; a_2X_2 to a_nX_n represent the m number of Q loads; and m is $n - 1$.

The aim of performing reliability analysis is to determine the structure's reliability index β, which is defined as an objective measure of safety associated with a limit state function. It is computed by dividing the mean value E[M] of the limit state function by its standard deviation D[M] as follows [30]:

$$\beta = \frac{E[M]}{D[M]} = \frac{\mathbf{a^T}E[\mathbf{X}]}{\sqrt{\mathbf{a^T}\mathrm{Cov}[\mathbf{X}, \mathbf{X^T}]\,\mathbf{a}}}. \tag{3}$$

The probability of failure is expressed as [31]:

$$P_f = \Phi(-\beta), \tag{4}$$

and the limit state function for fatigue of steel railway bridges can be expressed as [32]:

$$M = (S^3N)_R^{1/3} - \sum_{i=1}^{m}(S^3N)_{Qi}^{\frac{1}{3}}, \tag{5}$$

where $(S^3N)_R^{1/3}$ is the resistance fatigue parameter; and $(S^3N)_Q^{1/3}$ is the load fatigue parameter.

The fatigue parameter for resistance, S^3N, for riveted details (Category D) is termed coefficient A from the literature and its statistics are obtained as shown in Table 1 [33]. The load fatigue parameter, $(S^3N)_{Qi}^{1/3}$ is further simplified to $(SN^{1/3})_{Qi}$ to compute its statistical parameters. N_Q is a deterministic parameter and represents the total number of live load cycles. S_Q is a random variable corresponding to equivalent stress ranges from m loads. Both load parameters are established from railway bridge monitoring data.

3.1. Computation of stress range and number of cycles

To determine the load fatigue parameter, stress ranges and cycle numbers are extracted from estimated strain response at the unmeasured locations using a rainflow counting algorithm, with stresses being determined from uniaxial strains multiplied by nominal Young's modulus (200 GPa) using Hooke's law [34]. The equivalent stress range S_{re}, is subsequently computed using the root-mean-cubed method as recommended in the American Railway Engineering and Maintenance of Way Association (AREMA) *Manual for Railway Engineering* [35], which appears as follows:

$$S_{re} = \sqrt[3]{\frac{\sum_i S_{ri}^3 N_i}{\sum_i N_i}} = \sqrt[3]{\sum_i^N p_i S_{ri}^3}, \tag{6}$$

where N_i is the number of cycles at the i^{th} stress range, S_r; $\sum_i N_i$ is the total sum of the number of cycles; and p_i is the fraction of the number of cycles at the i^{th} stress range to the total number. Fig. 13 shows a

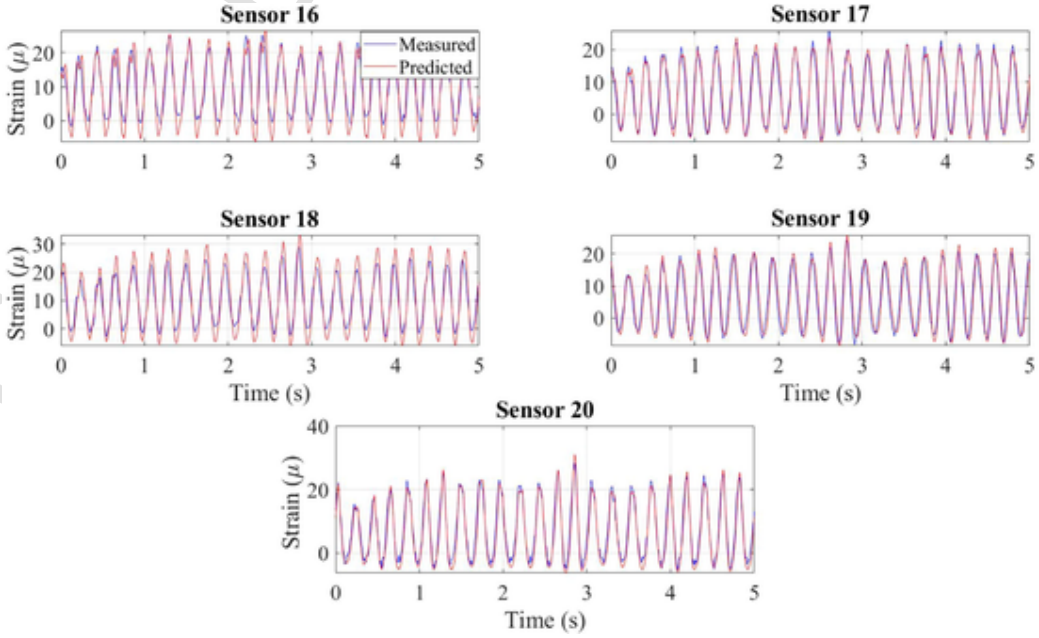

Fig. 12. SOM classification: predicted and measured strain time-histories for Class 1 (light) train passages on Track 2, Sensors 16 – 20.

Table 1
Fatigue resistance statistical parameters [33].

	Mean Fatigue, A	COV
Slope m = 3 for stress range ≤ 10 ksi (68.9 MPa)	98×10^8	20.3%

representative equivalent stress range histogram computed from predicted strain response at the first unmeasured location, Sensor 16, using RMS and k-means clustering.

To estimate statistical parameters for S_Q, an appropriate parametric distribution should be fit to the equivalent stress range. However, it is difficult to choose an appropriate parametric distribution that can suitably fit the histogram in Fig. 13, which represents stress ranges obtained from estimated strains at Sensor 16. Due to this challenge, KDE was utilized to estimate statistical parameters. It is noteworthy to mention that Sensor 16 data is representative of all unmeasured sensor locations in the red box in Fig. 3.

3.1.1. Equivalent stress range with KDE

KDE is used to determine a dataset's underlying probability density function. KDE does not require the assumption that underlying data belongs to a parametric family and has a wide range of applications and extensions, thereby making it a popular non-traditional estimator of univariate and multivariate densities [36]. KDE automatically learns the shape of the density curve from the data, and its non-traditional nature makes it a preferred method for data from an unknown distribution [37].

KDE calculates the probability density function of a random variable from an unknown distribution for any real value of x as follows:

$$\hat{f}_h(x) = \frac{1}{m}\sum_{i=1}^{m} K_h(x - x_i) = \frac{1}{mh}\sum_{i=1}^{m} K\left(\frac{x - x_i}{h}\right) \tag{7}$$

where $x_1, x_2, \cdots, x_m$ are random samples from an unknown distribution; m is the sample size; h is the bandwidth; and $K(.)$ is the kernel smoothing function. As shown in the literature, a range of smoothing functions such as normal, uniform, triangular, and Epanechnikov can be used [38].

KDE is calculated by weighting distances of each random variable sample from a particular point x. These weighted distances are then summed to compute a final density estimate. The more samples around point x, the higher the final density estimate. For each kernel, the mean value and standard deviation correspond to the random variable's observation and bandwidth, respectively.

The choice of bandwidth plays a vital role in the smoothness of the density curve. A narrow bandwidth (i.e., lower standard deviation) produces a jagged curve, indicating undersmoothing, whereas a wide bandwidth (i.e., higher standard deviation) produces extreme smoothing, hiding important data features. Numerous approaches for determining an optimal bandwidth are reported in the literature. Silverman's rule of thumb was selected for the current study because of its robustness and ease of implementation [39]:

$$h = 0.9 \min\left(\sigma, \frac{IQR}{1.34}\right) m^{-1/5} \tag{8}$$

where σ is the standard deviation of the random variables; IQR is the inter-quartile range of the random variables; and m is the number of variables.

Using Silverman's rule of thumb as given in Eqn. (8), an optimal bandwidth of 0.1641 MPa (0.0238 ksi) was determined for the equivalent stress range at Sensor 16 and subsequently utilized to estimate the density function with Eqn. (7). Fig. 14 depicts the resulting density function, which was observed to appropriately fit the equivalent stress range distribution histogram at Sensor 16. Equivalent stress ranges at other unmeasured locations and their corresponding KDE density functions are found in the Appendix.

The selected, optimal, KDE bandwidth corresponds to the standard deviation of the equivalent stress range (loads) while each sample/observation in the equivalent stress range is taken as the mean value for that load. Hence, each equivalent stress range observation is characterized by its mean and standard deviation corresponding to its value and bandwidth respectively.

3.1.2. Number of stress cycles

The extracted number of cycles from predicted strains (i.e., classification based on RMS and k-means clustering) at Sensor 16 for monitored train passages was 4,638,783. Since these cycles do not account for the entire number of stress cycles experienced by the bridge since it opened, a conservative assumption was made to establish the total number of accumulated stress cycles [40]. Following publication of the first AREMA design specifications for steel railroad bridges in 1905, it was widely believed that design and rating capacities for bridges based on the Cooper E series design load doubled over the following decades. Consequently, demand (measured as weight per car) skyrocketed con-

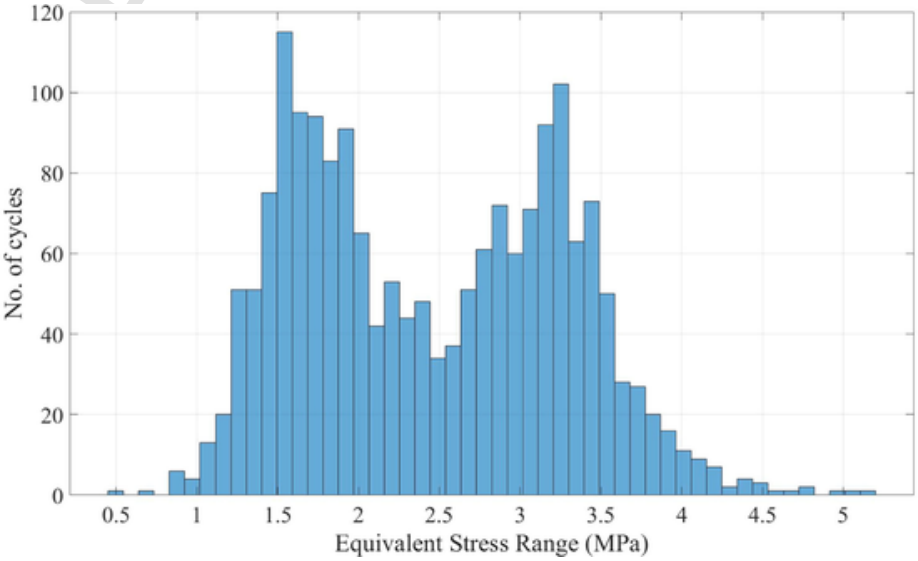

Fig. 13. Equivalent stress range at Sensor 16 using estimated strains and RMS.

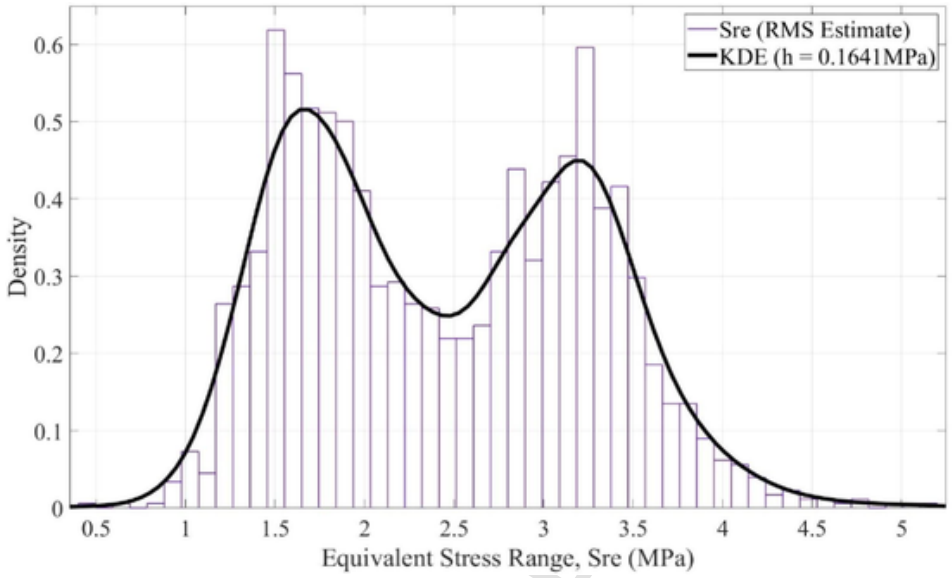

Fig. 14. Equivalent stress range at Sensor 16 characterized using KDE (h = 0.1641 MPa).

current with capacity expansion, and soon met the increased bridge's capacity [41,42]. Hence, it was assumed that capacity limits for older bridges had been reached. Although the gap between capacity and demand has narrowed or been exceeded, loads have not increased recently and are not expected to in the near future [41].

Therefore, it is reasonable to assume that applied load magnitudes on the bridge were lower than or largely constant to the demand (applied loads) during the monitoring period. Thus, equivalent stress ranges calculated from monitoring data were assumed to be a fair reflection of past and future loading regimes. The number of cycles before failure was considered a function of time and it was assumed that the number of cycles would increase by r per year after the bridged opened, due to the continuous and increasing use of the bridge over time. Hence, the total accumulated number of cycles per year, $N_t(y)$, is expressed as follows:

$$N_t(y) = \frac{N_{t,\,data}\frac{12}{2}}{(1+r)^{100}} * \left[\frac{(1+r)^y - 1}{r}\right] \tag{9}$$

where: y is the number of years after bridge opening year; $N_{t,data}$ is the total accumulated stress cycles from the two-month monitoring data; and r is the increase rate.

The resulting total and cumulative number of stress cycles per year for a 200-year period after the bridge opened is shown in Fig. 15. Cumulative stress cycles per year correspond to the total number of cycles due to live loads, N_Q, defined earlier. When compared to cumulative stress cycles computed from measured response, stress cycles from predicted response were slightly higher (2.6%) during the monitoring period and for the 200-year period. Cumulative stress cycles at other unmeasured locations are found in the Appendix.

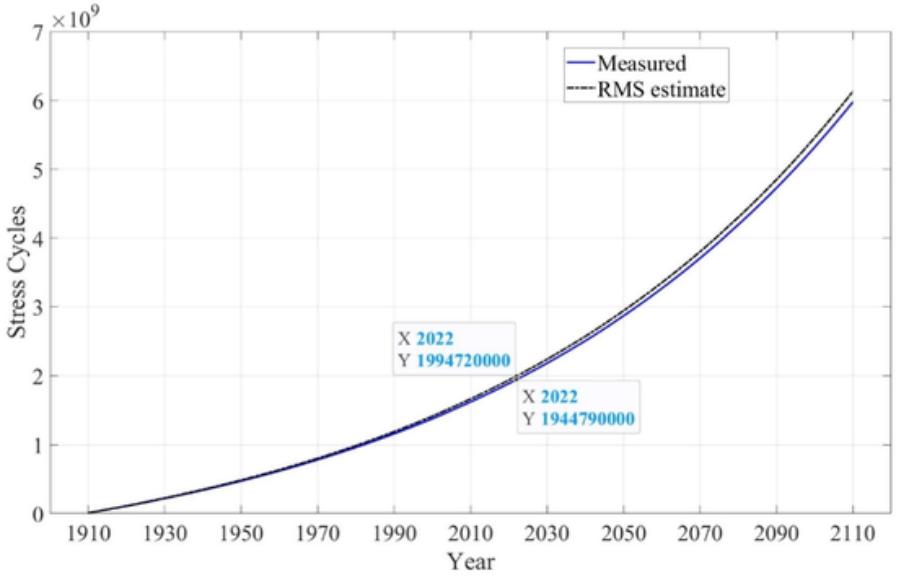

Fig. 15. Classification using RMS – cumulative stress cycles from predicted and measured strain time-histories at Sensor 16.

3.2. Reliability index

After obtaining fatigue load parameters, N_Q, per year and S_{Qi} from monitoring data at each unmeasured location (Sensors 16–20), fatigue reliability indices were computed over the period of interest using Eqn. (3). It was deemed permissible to utilize equivalent stress ranges calculated from monitoring data as a suitable representation of past and future responses since bridge load demands before the monitoring period were presumed to be less than or equal to demands during the monitoring period [40].

The constant vector $\mathbf{a} = [a_1, a_2, a_3, \cdots, a_n]$, in Eqn. (3) corresponds to the number of stress cycles, N, from Eqn. (5). a_1 is a constant fatigue resistance parameter value and $a_2 : a_n$ correspond to constants associated with each load parameter m, where $m = n - 1$. Consequently, a_1 is taken to be 1 since the fatigue resistance, S^3N, has been evaluated and its statistics are available as presented in Table 1 [33]. As a result, $a_2 : a_n$ are taken as the cumulative number of stress cycles $N_t(y)$ at load parameter year y.

Similarly, the mean of variable vector $\mathbf{E}[\mathbf{X}] = \left[\mu_R; \mu_{Q_1}; \mu_{Q_2}; \cdots; \mu_{Q_m}\right]^T$ in Eqn. (3) corresponds to the mean of the equivalent stress range for the fatigue limit state expressed in Eqn. (5). The cube root of the mean value presented in Table 1 is calculated to be 2140 ksi and taken as μ_R while $\mu_{Q_1}, \mu_{Q_2}, \mu_{Q_3}, \cdots, \mu_{Q_m}$ correspond to equivalent stress ranges $S_{re1}, S_{re2}, S_{re3}, \cdots, S_{rem}$.

The covariance matrix of the random variable vector, $\mathrm{Cov}[X, X^T]$, corresponds to the covariance of the equivalent stress range. The $n \times n$ matrix provides covariance between each pair of elements i, j of the random vector. Its main diagonal contains the variance of each element i with respect to itself, where $i = 1, 2, 3, \cdots, n$. Assuming no correlation between resistance and load parameters, all covariance matrix values are taken as zero ($X_{ij} = 0$ where $i \neq j$) except for those on the main diagonal. The first diagonal value corresponds to a resistance variance of $X_{11} = \sigma_r^2 = 208^2$, while other diagonal values correspond to load variances ($X_{22}, X_{33}, \cdots, X_{nn} = \sigma_q^2$) taken to be the square of the KDE bandwidth (i.e., 0.1641^2) at Sensor 16.

It is noteworthy to mention that reliability analyses presented herein are limited to instrumented bridge components (i.e,. each sensor location). Establishing accurate system reliabilities are beyond the scope of this study since sensors are not placed at the connections. However, the proposed KDE and virtual sensing approach can still be used to determine system reliability. Interested readers are referred to well cited system reliability publications [40,43].

4. Results and discussion

After parameters described above were computed, reliability indices were determined for the period of interest. Results for Sensor 16 are initially presented with estimated indices found using estimated strains classified using both RMS and SOM. Resulting reliability indices from estimated strain responses at Sensor 16 were compared against corresponding indices from measured strain response as shown in Fig. 16. Reliability indices from estimated strain responses using both classification methods were observed to be in good agreement with corresponding indices from the measured responses. In general, the predicted reliability indices from measured and estimated response over the period of interest exceed the current AREMA practice for fatigue evaluation corresponding to Minimum Life (reliability index of 2) [33]. This result indicates that the bridge components continue to perform well in terms of resistance against crack initiation and can be considered suitable for further service during the period of interest.

Differences between estimated and measured indices did progressively increase over the 200 years of interest, with reliability indices from estimated responses using both classification methodologies being less conservative than indices based on field measurements. The maximum differences between estimated and measured reliability indices were approximately 0.14 and 0.16 for RMS and SOM estimates, respectively, which was deemed acceptable. It is worth noting that since the cumulative number of cycles from predicted strains were higher than those from measured strains (as shown in Fig. 15), one would expect lower estimated strain reliability indices than those from the measured strains. However, as illustrated in Fig. 16, the opposite trend was observed. Reliability indices from estimated strains were observed to be higher than those from measured strains. This observation can be justified and attributed to the influence using the equivalent stress range as the random variable when computing the reliability index.

Similar procedures were followed to determine reliability indices at other unmeasured locations for the period of interest. Fig. 17 compares estimates using the two classification methodologies to measured in-

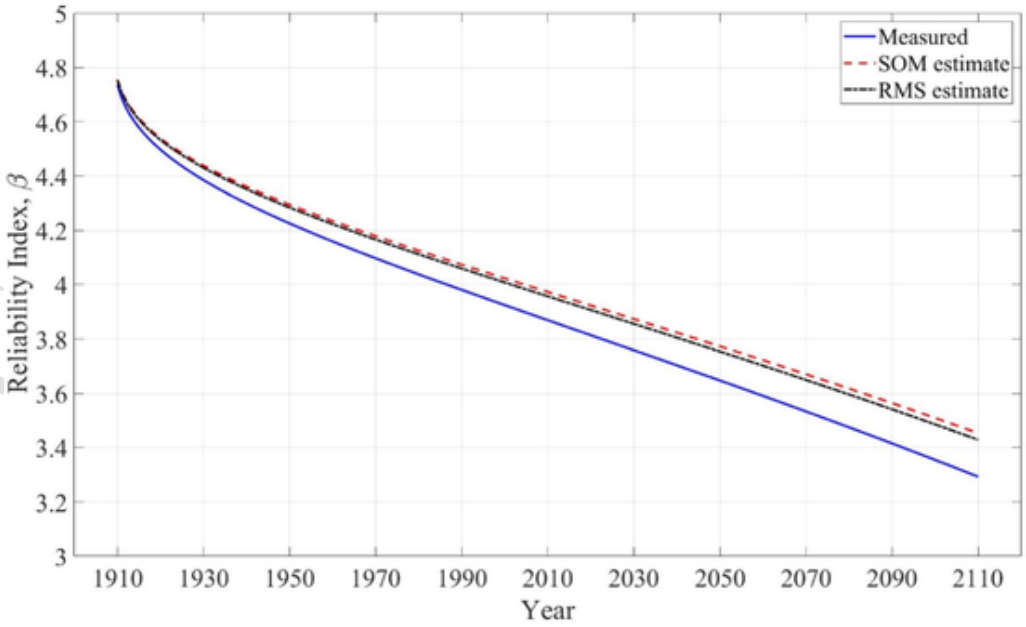

Fig. 16. Reliability indices using RMS and SOM estimated and measured strains, Sensor 16.

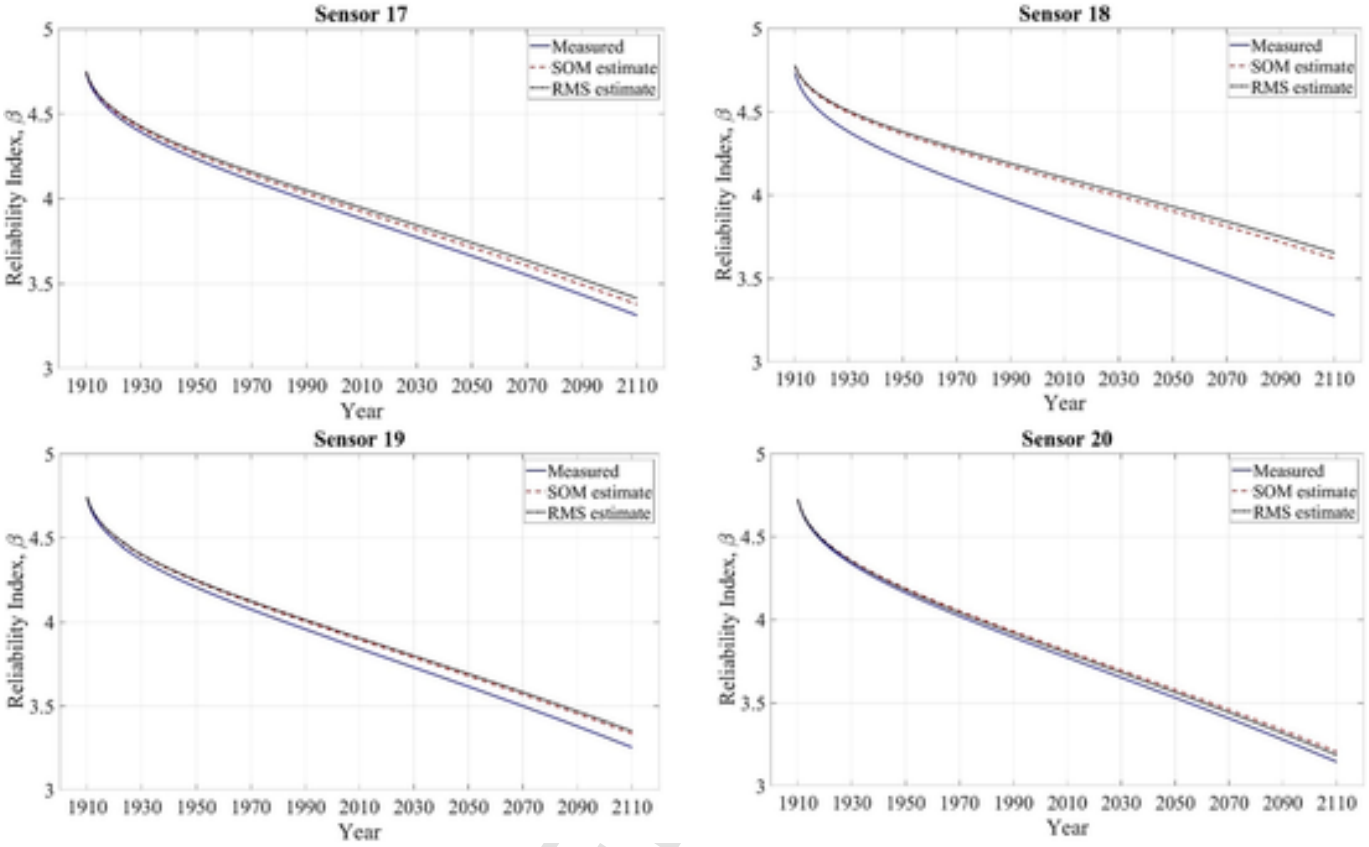

Fig. 17. Reliability indices using RMS and SOM estimated and measured strains, Sensors 17 – 20.

dices over the 200-year period. Similar trends to Sensor 16 were observed, except for Sensor 18. Observed differences for Sensor 18 were potentially attributed to sensor data quality throughout the monitoring period. The data quality could have been affected by sensor placement and/or position.

For the remaining sensors, reliability indices computed from estimated responses were consistently acceptably close to indices based on measured responses. This potentially reduces risks associated with inaccurately identifying areas of concern for fatigue. Estimated results were generally similar irrespective of classification method, but agreement did differ slightly between sensors. SOM classification provided more accurate indices for Sensors 17 – 19 while RMS did so for Sensors 16 and 20. It should be noted that classification using SOM was more efficient computationally than RMS, even though labeling results according to track location and load categories was shown to be less accurate as discussed earlier. To further evaluate and quantitatively compare estimation quality, three common mean error methods were employed to assess levels of error between estimated and measured reliability indices.

4.1. Mean error methods

a. Mean Squared Error (MSE)

MSE is the average squared distance between actual and predicted values [44] and varies between zero and infinity. A larger MSE indicates that data points are widely dispersed around the mean. Conversely, a lower MSE implies smaller errors, less dispersion, and consequently better predictions. MSE is expressed as follows:

$$MSE = \frac{1}{n}\sum_{i=1}^{n}\left(\beta_i - \widehat{\beta}_i\right)^2, \tag{10}$$

where β_i is the actual reliability index value from measured strain response; $\widehat{\beta}_i$ is the corresponding reliability index value from estimated strain response; and n is the number of years/observations.

b. Mean absolute error (MAE)

MAE is the average of the absolute difference between estimated and true data values [45]. It is expressed as follows:

$$MAE = \frac{1}{n}\sum_{i=1}^{n}\left|\left(\beta_i - \widehat{\beta}_i\right|\right|, \tag{11}$$

where β_i is the actual reliability index value from measured strain response; $\widehat{\beta}_i$ is the corresponding reliability index value from estimated strain response; and n is the number of years/observations.

c. Coefficient of determination R^2

The coefficient of determination is the mean squared error normalized with respect to the variance [46,47]. The coefficient of determination is based on the correlation between actual and predicted values. Its values lie between 0 and 1 with 1 implying perfect correlation and is expressed as follows:

$$R^2 = 1 - \frac{MSE}{Var\left(\beta_i\right)}, \tag{12}$$

where MSE is the mean squared error; and β_i is the actual reliability index value from measured strain response.

Results from these quality metric calculations are listed in Table 2. They indicate that RMS has larger MSE and MAE values, implying greater error than SOM. Both classification methods have high R^2 values indicating good correlation to actual response indices, except at Sensor 18, as expected. Based on these results, both methods could be used interchangeably but SOM classification is recommended based on lower MAE and MSE values and the aforementioned computational benefits.

5. Conclusions

In this study, probabilistic fatigue assessment was performed via reliability analysis using estimated strain response at select, unmeasured, locations on a monitored railway bridge. Prior to fatigue assessment, two classification methods, RMS with k-means clustering and SOM, were utilized to categorize stain time histories from train passages into train groups traveling in a similar direction and groups of similar total load. The purpose of the classification was to reduce POM variability resulting from varying loads and locations during monitoring. Following classification, strain response was estimated at unmeasured locations using a data driven SVD method. A reliability analysis methodology was utilized, one that employed kernel density estimation (KDE) to appropriately fit the equivalent stress range distribution, to perform fatigue assessment. To assess proposed methodology accuracy, unmeasured results were compared to results obtained from sensors placed at those locations.

Results from the study indicated that:

- Reliability-based fatigue assessment employing KDE eliminates difficulties associated with selecting appropriate probability distributions and resulted in more accurate predictions.
- Reliability indices from estimated strain response using both classification approaches closely matched corresponding indices from actual, measured response at the unmeasured locations (i.e., Sensors 16 to 20). Reliability indices from estimated response were slightly higher than corresponding indices from measured response.
- Reliability indices from estimated response classified using SOM appeared to generally provide better prediction than those classified using RMS. Classification using SOM produced a lower range of MAE and MSE and is more computationally efficient thus, making preferable when compared to classification using RMS.

It is important to mention that the novelty of this research relates to dealing with non-Gaussian or arbitrary equivalent stress range distributions obtained from actual or estimated strain response. In a follow-up study, a FE model will be developed to estimate stress concentrations at the connections using measured strain responses at the stringer-to-floor-beam locations.

Table 2
Error metric for classification methodologies.

	Classification	Sensor 16	Sensor 17	Sensor 18	Sensor 19	Sensor 20
MSE	RMS	0.0084	0.0046	0.0646	0.0043	7.5170e-04
	SOM	0.0117	0.0019	0.0532	0.0030	0.0017
MAE	RMS	0.0865	0.0639	0.2402	0.0617	0.0259
	SOM	0.1021	0.0415	0.2179	0.0516	0.0387
R^2	RMS	0.9351	0.9637	0.5088	0.9685	0.9951
	SOM	0.9096	0.9847	0.5958	0.9780	0.9891

CRediT authorship contribution statement

Emmanuel Akintunde : Conceptualization, Software, Visualization, Data curation, Investigation, Writing – original draft, Validation. **Saeed Eftekhar Azam :** Conceptualization, Writing – review & editing, Data curation, Investigation, Validation. **Daniel G. Linzell :** Conceptualization, Writing – review & editing, Supervision, Funding acquisition.

Declaration of Competing Interest

The authors declare the following financial interests/personal relationships which may be considered as potential competing interests: Daniel Linzell reports financial support was provided by National Science Foundation.

Data availability

The authors do not have permission to share data.

Acknowledgments

The authors would like to acknowledge support provided by NSF Award #1762034 BD Spokes: MEDIUM: MIDWEST: Smart Big Data Pipeline for Aging Rural Bridge Transportation Infrastructure (SMARTI). The authors also gratefully acknowledge the assistance, access, computing resources, data, and expertise provided by the University of Nebraska's Holland Computing Center, Union Pacific Railroad Company, and Bridge Diagnostics Inc. in association with this project.

Appendix.

The appendix contains results for:

1. Equivalent stress ranges at unmeasured locations (Sensor 16—20) calculated using estimated and measured strains.
2. Cumulative stress cycles at unmeasured locations (Sensor 16—20) calculated using estimated and measured strains.

1. **Equivalent stress range at unmeasured locations**
See Figs. A1–A10.
2. **Cumulative stress cycles at unmeasured locations**
See Figs. A11-A14.

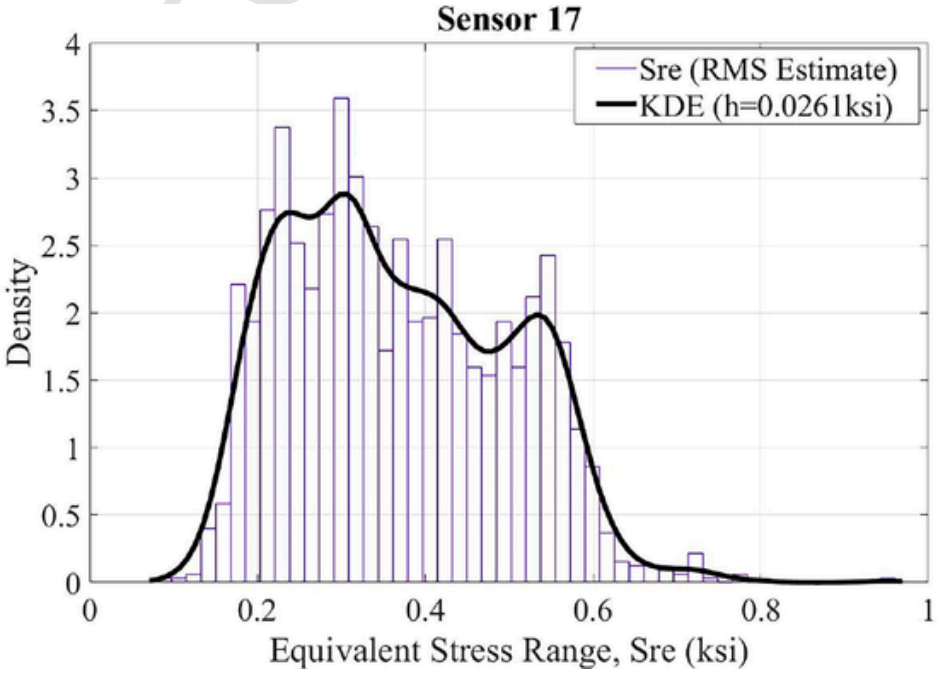

Fig. A3. Equivalent stress range at Sensor 17 using RMS estimated strains characterized using KDE (h = 0.0261 ksi).

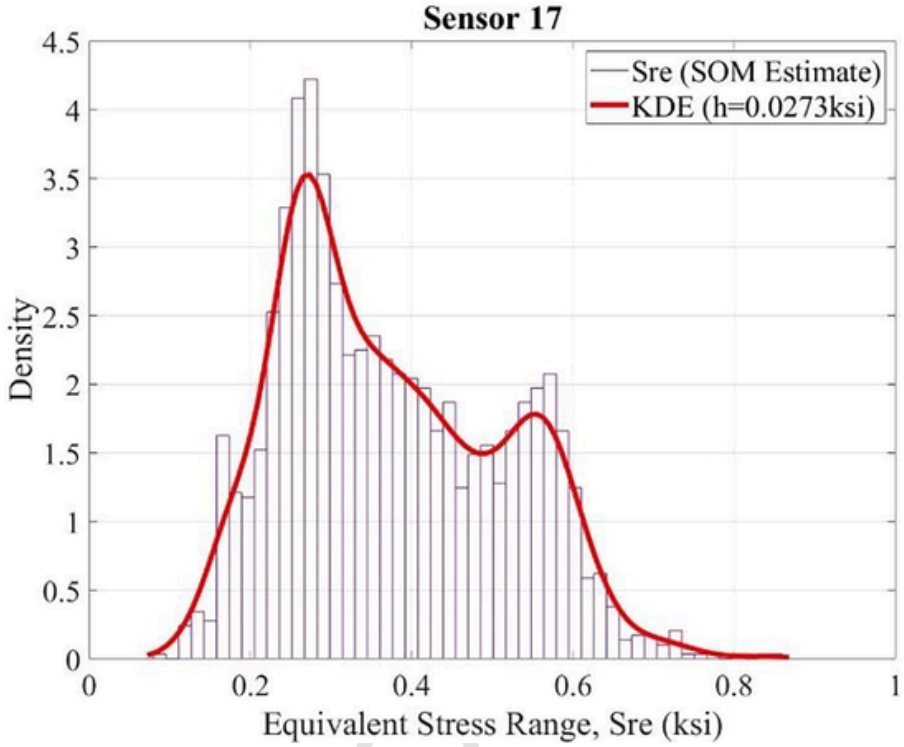

Fig. A4. Equivalent stress range at Sensor 17 using SOM estimated strains characterized using KDE (h = 0.0273 ksi).

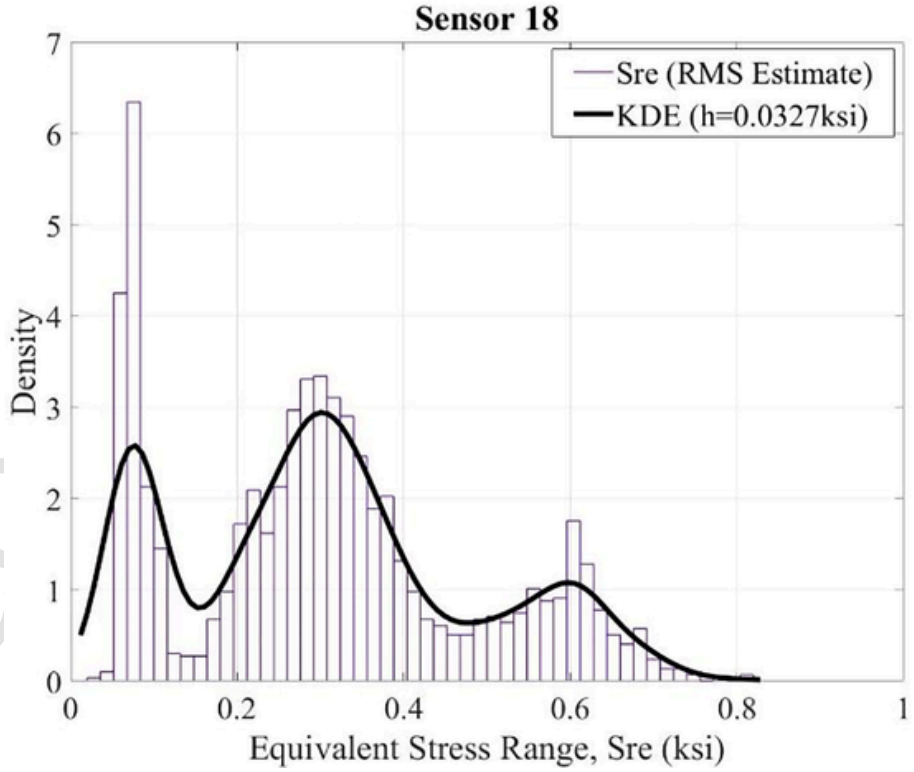

Fig. A5. Equivalent stress range at Sensor 18 using RMS estimated strains characterized using KDE (h = 0.0327 ksi).

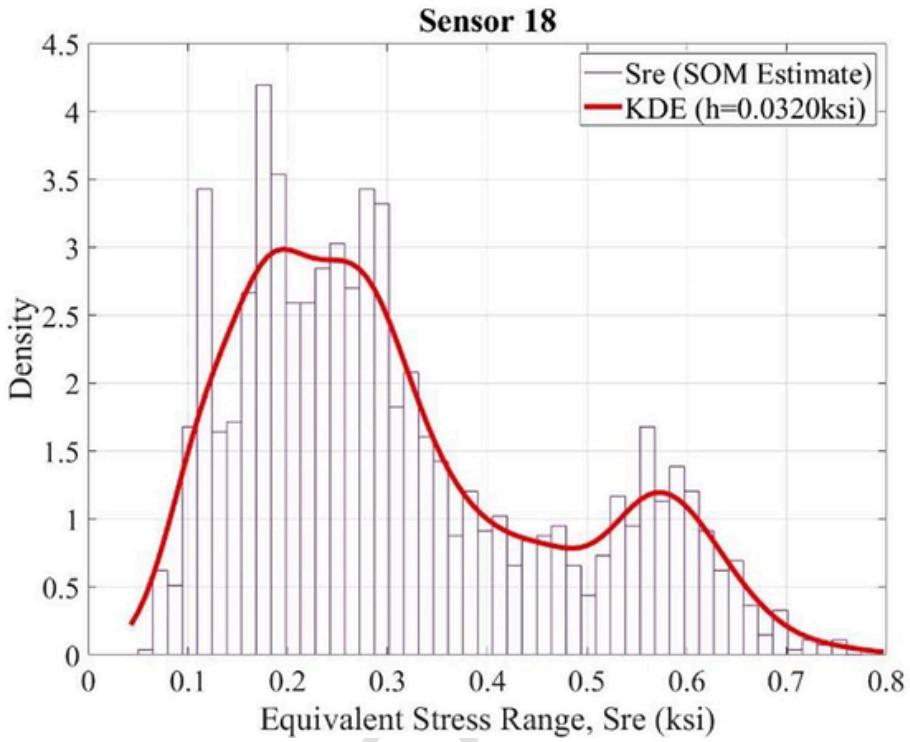

Fig. A6. Equivalent stress range at Sensor 18 using SOM estimated strains characterized using KDE (h = 0.0320 ksi).

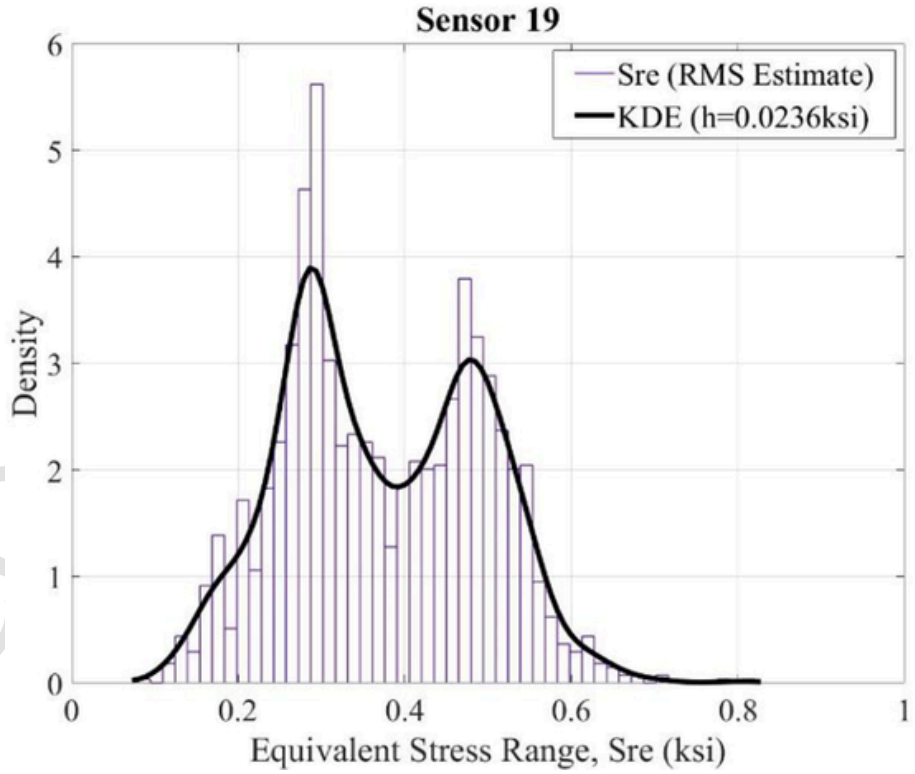

Fig. A7. Equivalent stress range at Sensor 19 using RMS estimated strains characterized using KDE (h = 0.0236 ksi).

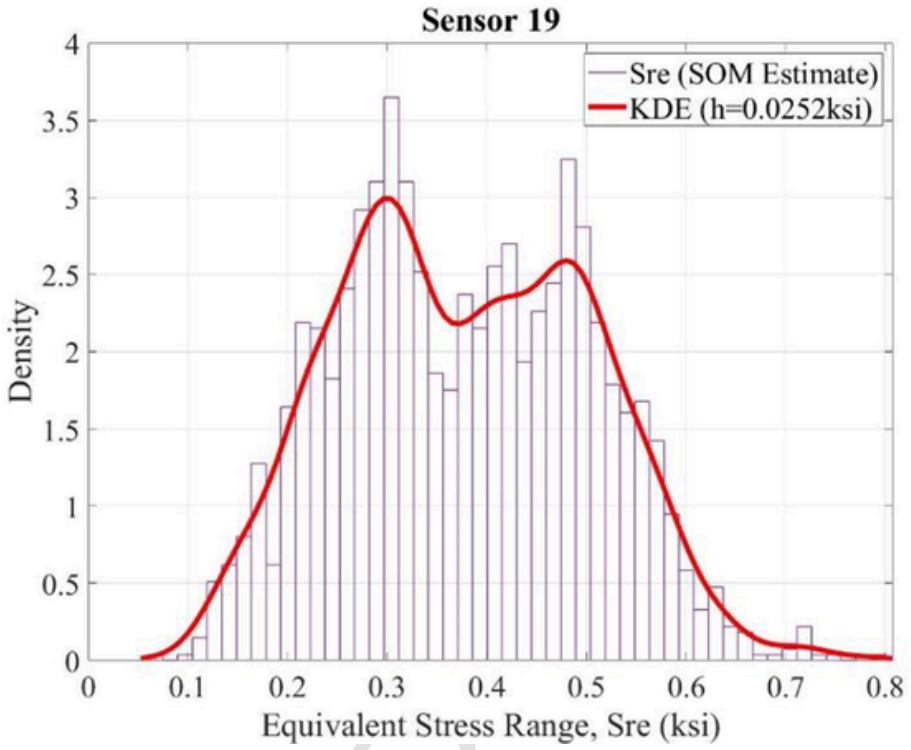

Fig. A8. Equivalent stress range at Sensor 19 using SOM estimated strains characterized using KDE (h = 0.0252 ksi).

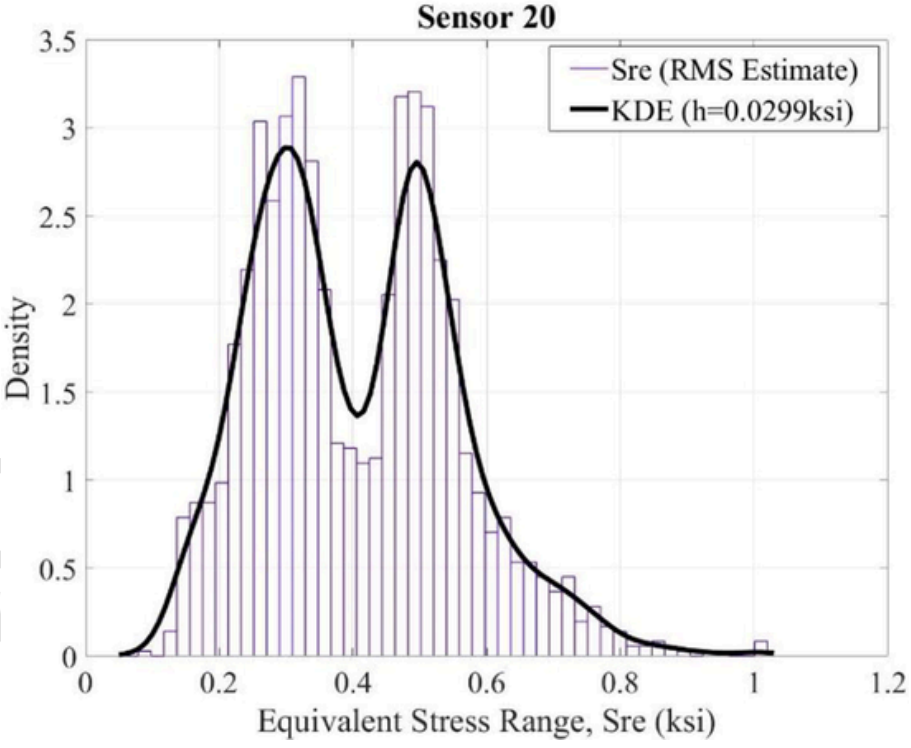

Fig. A9. Equivalent stress range at Sensor 20 using RMS estimated strains characterized using KDE (h = 0.0299 ksi).

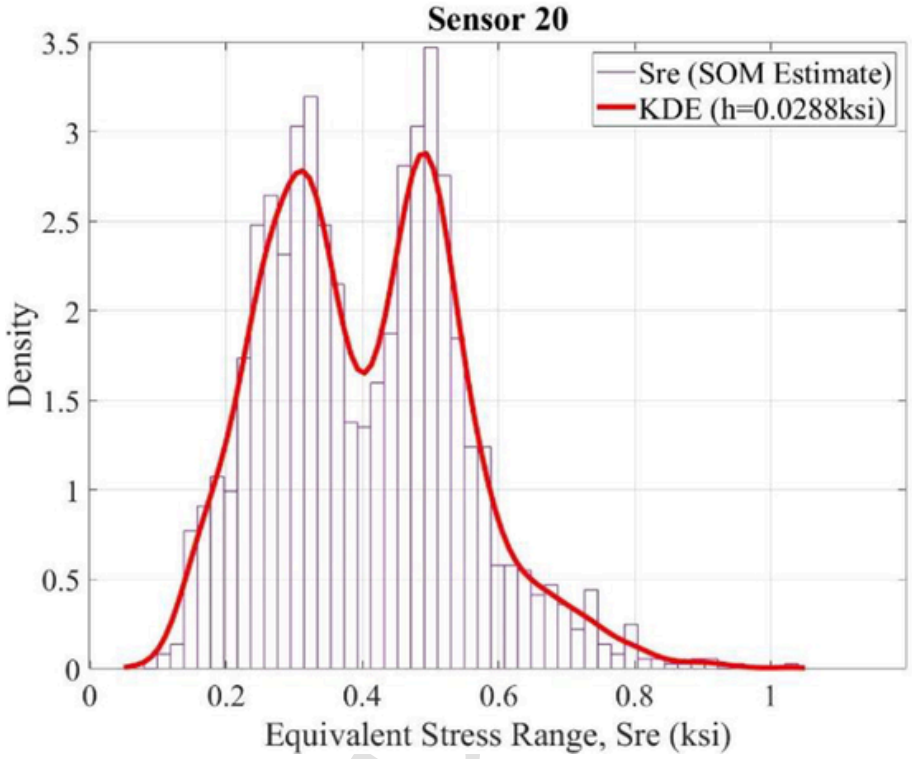

Fig. A10. Equivalent stress range at Sensor 20 using SOM estimated strains characterized using KDE (h = 0.0288 ksi).

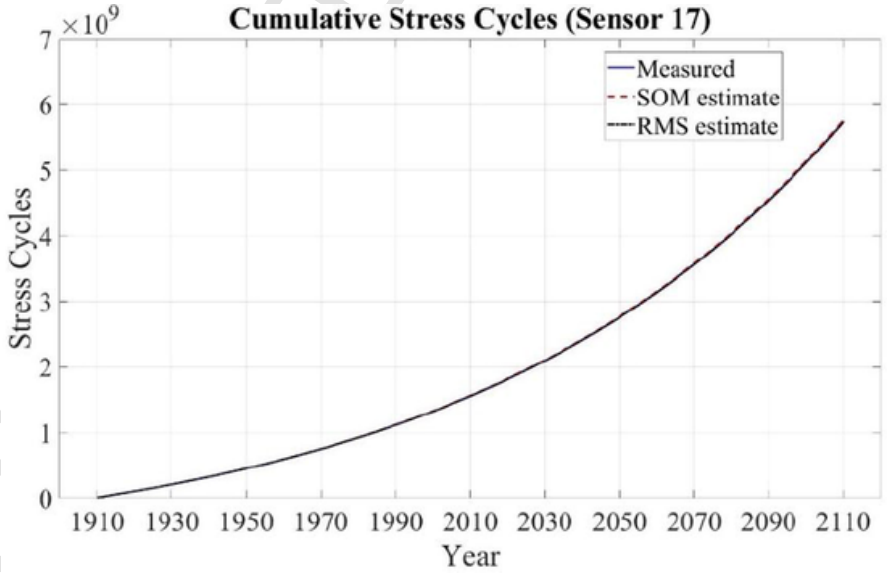

Fig. A11. Cumulative stress cycles from predicted and measured strain time-histories at Sensor 17.

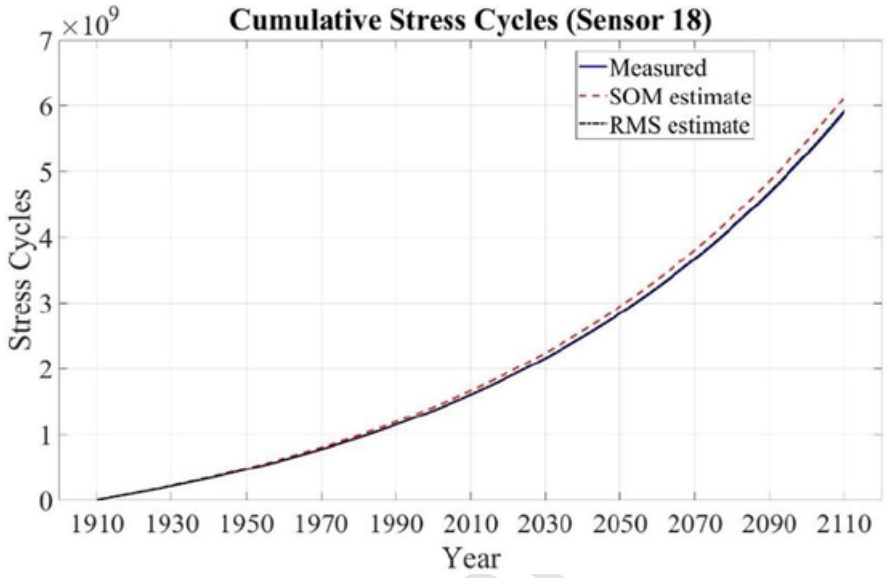

Fig. A12. Cumulative stress cycles from predicted and measured strain time-histories at Sensor 18.

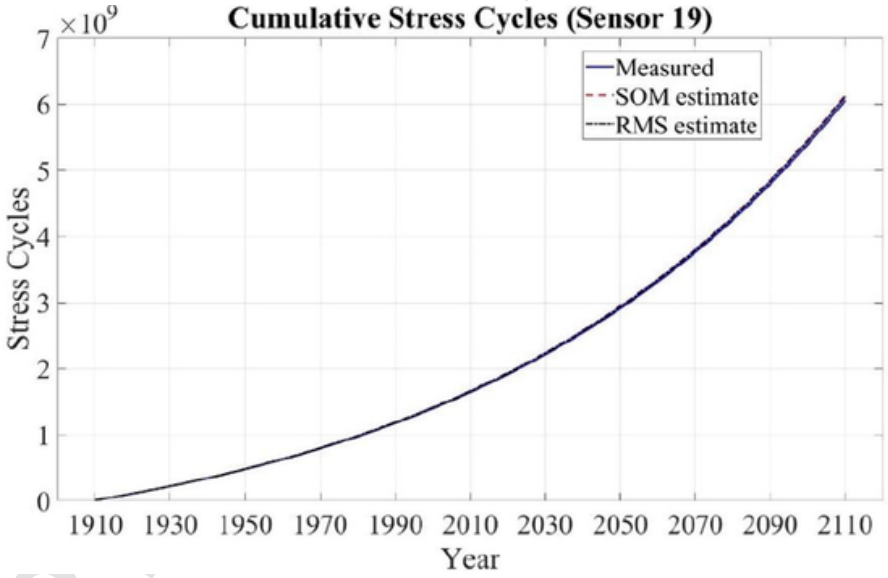

Fig. A13. Cumulative stress cycles from predicted and measured strain time-histories at Sensor 19.

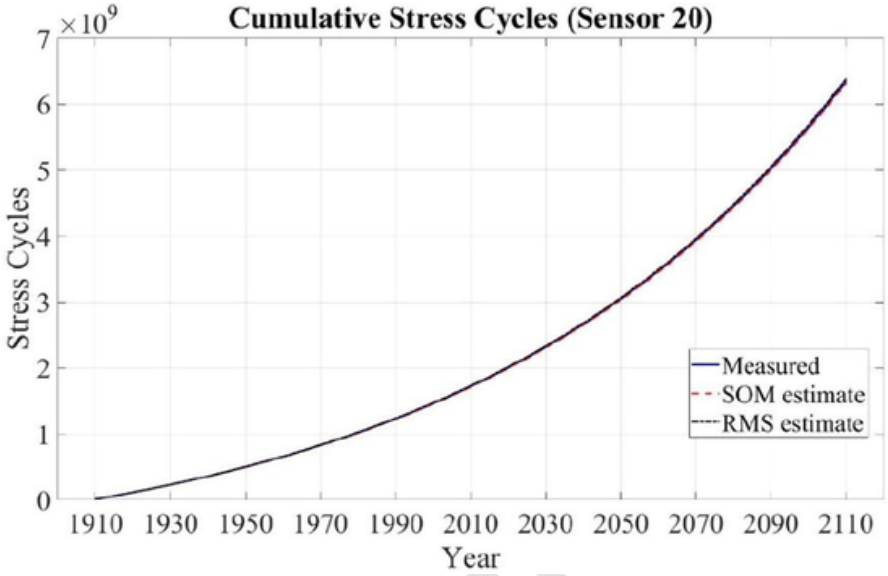

Fig. A14. Cumulative stress cycles from predicted and measured strain time-histories at Sensor 20.

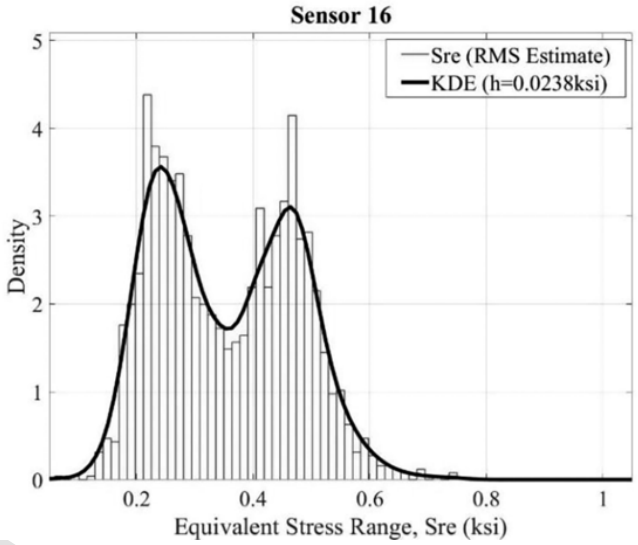

Fig. A1. Equivalent stress range at Sensor 16 using RMS estimated strains characterized using KDE (h = 0.0238 ksi).

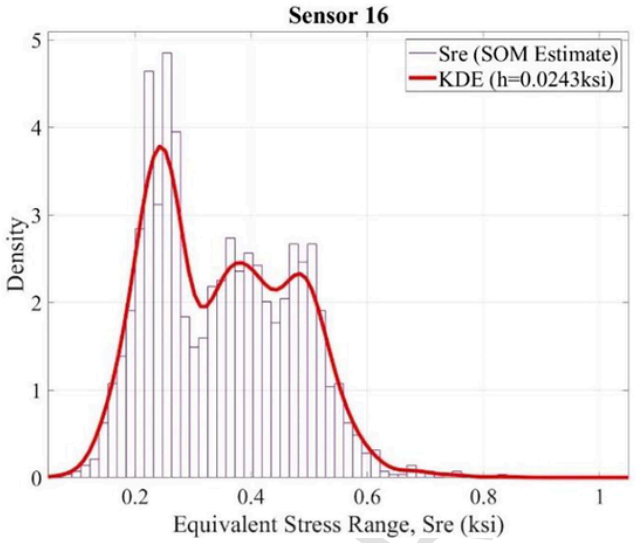

Fig. A2. Equivalent stress range at Sensor 16 using SOM estimated strains characterized using KDE (h = 0.0243 ksi).

References

[1] Tarpø M, et al. Expansion of experimental mode shape from operational modal analysis and virtual sensing for fatigue analysis using the modal expansion method. Int J Fatigue 2020;130:105280.
[2] Farrar C.R, Worden K. Structural health monitoring.: a machine learning perspective. John Wiley & Sons 2012.
[3] Ren P, Zhou Z. Strain response estimation for the fatigue monitoring of an offshore truss structure. Pac Sci Rev 2014;16(1):29–35.
[4] Ren P, Zhou Z. Strain estimation of truss structures based on augmented Kalman filtering and modal expansion. Adv Mech Eng, vol. 9, (11), pp. 1687814017735788, 2017.
[5] Palanisamy R, et al. Experimental validation of Kalman filter-based strain estimation in structures subjected to non-zero mean input. Smart Struct Syst 2015; 15(2):489–503.
[6] Lee G. Prediction of strain responses from the measurements of displacement responses. Mech Syst Sig Process 2007;21(2):1143–52.
[7] Tarpø M. Stress estimation of offshore structures. Aarhus University 2020. https://doi.org/10.7146/aul.393.
[8] Gelb A. Applied Optimal Estimation. MIT Press; 1974.
[9] Simon D. Optimal State Estimation: Kalman, H Infinity, and Nonlinear Approaches. John Wiley & Sons; 2006.
[10] Maes K, et al. Dynamic strain estimation for fatigue assessment of an offshore monopile wind turbine using filtering and modal expansion algorithms. Mech Syst Sig Process 2016;76:592–611.
[11] Noppe N, et al. Fatigue stress estimation of offshore wind turbine using a kalman filter in combination with accelerometers. In: Proceedings of International Conference on Noise and Vibration Engineering (ISMA 2018), International Conference on Uncertainty in Structural Dynamics (USD 2018), 2018.
[12] Pedersen M.W, et al. Examination of modal expansion and kalman filtering techniques for vibration estimation. 9th ECCOMAS Thematic Conference on Smart Structures and Materials. 2019.
[13] Deng H, et al. Modal learning displacement–strain transformation. Rev Sci Instrum 2019;90, (7):075113.
[14] Lu W, et al. Stress prediction for distributed structural health monitoring using existing measurements and pattern recognition. Sensors 2018;18, (2):419.
[15] Eftekhar Azam S, et al. Experimental validation and numerical investigation of virtual strain sensing methods for steel railway bridges. J Sound Vibrat, vol. 537, pp. 117207, 2022. Available: https://www.sciencedirect.com/science/article/pii/S0022460X2200400X. DOI: https://doi.org/10.1016/j.jsv.2022.117207.
[16] Akintunde E, Azam SE, Linzell DG. Singular value decomposition and unsupervised machine learning for virtual strain sensing: application to an operational railway bridge, (Under revision) .
[17] Eftekhar Azam S, Rageh A, Linzell D. Damage detection in structural systems utilizing artificial neural networks and proper orthogonal decomposition. Struct Control Health Monit 2019;26, (2):e2288.
[18] Kanungo T, et al. An efficient k-means clustering algorithm: Analysis and implementation. IEEE Trans Pattern Anal Mach Intell 2002;24(7):881–92.
[19] Fung G. A comprehensive overview of basic clustering algorithms. IEEE trans Inf Theory 2001;27(1):49–60.
[20] Rageh A, Linzell D.G, Azam S.E. Automated, strain-based, output-only bridge damage detection. J Civ Struct Heal Monit 2018;8(5):833–46.
[21] Tobias D.H, Foutch D.A, Choros J. Loading spectra for railway bridges under current operating conditions. J Bridge Eng 1996;1(4):127–34.
[22] Tobias D.H, Foutch D.A. Reliability-based method for fatigue evaluation of railway bridges. J Bridge Eng 1997;2(2):53–60.
[23] Rakoczy AM, Otter D, Dick SM. Effects of articulated double-stack cars on bridges. Technology Digest, 2017.
[24] Dick S, et al. Development of a fatigue load for railway bridges. No Rail Safety IDEA Project 2022;45:2022.
[25] Rakoczy A.M, Otter D.E, Dick S.M. Analytical and measured effects of short and heavy rail cars on railway bridges in the USA. Appl Sci 2021;11, (7):3126.
[26] Kohonen T. Essentials of the self-organizing map. Neural Netw 2013;37:52–65.
[27] Sajja P.S, Akerkar R. Bio-inspired models for semantic web. Swarm Intelligence and Bio-Inspired ComputationAnonymous. 2013.
[28] Kaski S. Data exploration using self-organizing maps. In: Acta Polytechnica Scandinavica: Mathematics, Computing and Management in Engineering Series no. 82, 1997, .
[29] MathWorks I. Cluster Data with a Self-Organizing Map. b 2021.
[30] Ditlevsen O, Madsen H.O. Structural Reliability Methods. Vol. 178. New York: Wiley; 1996.
[31] Nowak A.S, Collins K.R. Reliability of structures. CRC Press; 2012.
[32] Rakoczy A.M, Nowak A.S, Dick S. Fatigue reliability model for steel railway bridges. Struct Infrastruct Eng 2016;12(12):1602–13.
[33] Rakoczy A.M, Otter D, Dick S. Railroad bridge fatigue life estimation using the probabilistic method and new fatigue resistance for riveted details. Struct Infrastruct Eng 2020;16(3):381–93.
[34] Feynman RP, Leighton RB, Sands M. The Feynman Lectures on Physics, Vol. I: The New Millennium Edition: Mainly Mechanics, Radiation, and Heat; 20111.
[35] AREMA A. Chapter 15 - Steel Structures. In Manual for Railway Engineering; 2019.
[36] Kim J, Scott C.D. Robust kernel density estimation. J Mach Learn Res 2012;13(1): 2529–65.
[37] Chen Y. A tutorial on kernel density estimation and recent advances. Biostatistics & Epidemiology 2017;1(1):161–87.
[38] Hansen BE. Lecture notes on nonparametrics. Technical report, University of Wisconsin; 2009.
[39] Silverman B.W. Density Estimation for Statistics and Data Analysis. Vol. 26. CRC Press; 1986.
[40] Flanigan KA, Lynch JP, Ettouney M. Probabilistic fatigue assessment of monitored railroad bridge components using long-term response data in a reliability framework. Structural Health Monitoring, pp. 1475921720915712, 2020.
[41] Moreu F, Spencer Jr BF. Framework for consequence-based management and safety of railroad bridge infrastructure using wireless smart sensors (WSS). Newmark Structural Engineering Laboratory Report Series, 2015.
[42] Unsworth J.F. Design and construction of modern steel railway bridges. CRC Press; 2017.
[43] Rakoczy A.M. Development of system reliability models for railway bridges. The University of Nebraska-Lincoln; 2012.
[44] Bendat J.S, Piersol A.G. Random data: analysis and measurement procedures. John Wiley & Sons; 2011.
[45] Everitt B.S, Skrondal A. The Cambridge dictionary of statistics. 4th ed. Cambridge, NY: Cambridge University Press; 2010.
[46] Hansen P.C, Pereyra V, Scherer G. Least squares data fitting with applications. JHU Press 2013.
[47] Lawson C.L, Hanson R.J. Solving least squares problems. Society for Industrial and Applied Mathematics 1995.